Electronic Supplementary Material (ESI) for RSC Advances.

Catecholase activity, DNA binding and Cytotoxicity studies of a Cu(II) complex of a pyridoxal Schiff base: Synthesis, X-ray crystal structure, spectroscopic, electrochemical and theoretical studies

Piyali Adak,[a] Bipinbihari Ghosh,[a] Antonio Bauzá,[b] Antonio Frontera,[b*] Alexander J. Blake,[c] Montserrat Corbella,[d] Chitrangada Das Mukhopadhyay[e] and Shyamal Kumar Chattopadhyay[a*]

[a] Department of Chemistry, Indian Institute of Engineering Science and Technology, Shibpur, Howrah 711 103, India, Fax: +91 033 2668 2916; e-mail: shch20@hotmail.com

[b] Department of Chemistry, University of the Balearic Islands, Carretera de Valldemossa km 7.5, 07122 Palma de Mallorca, IllesBalears, Spain

[c]School of Chemistry, The University of Nottingham, University Park, Nottingham NG7 2RD, U.K.

[d]Department of Inorganic Chemistry, University of Barcelona, MartíiFranquès 1-11, 08028 Barcelona, Spain

[e]Centre for Healthcare Science and Technology, Indian Institute of Engineering Science and Technology, Shibpur, Howrah 711 103, India

Contents	Page no.

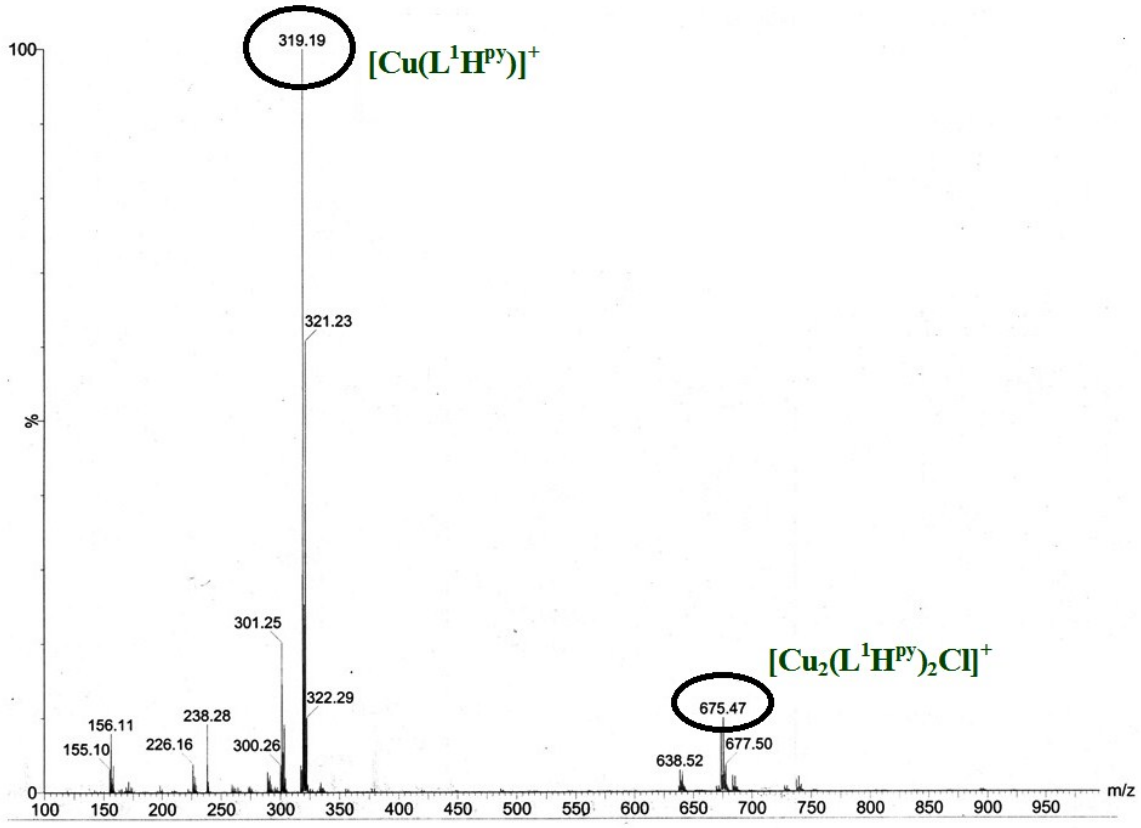

Figure S1: Mass spectrum(in positive mode) of **1** in methanol.

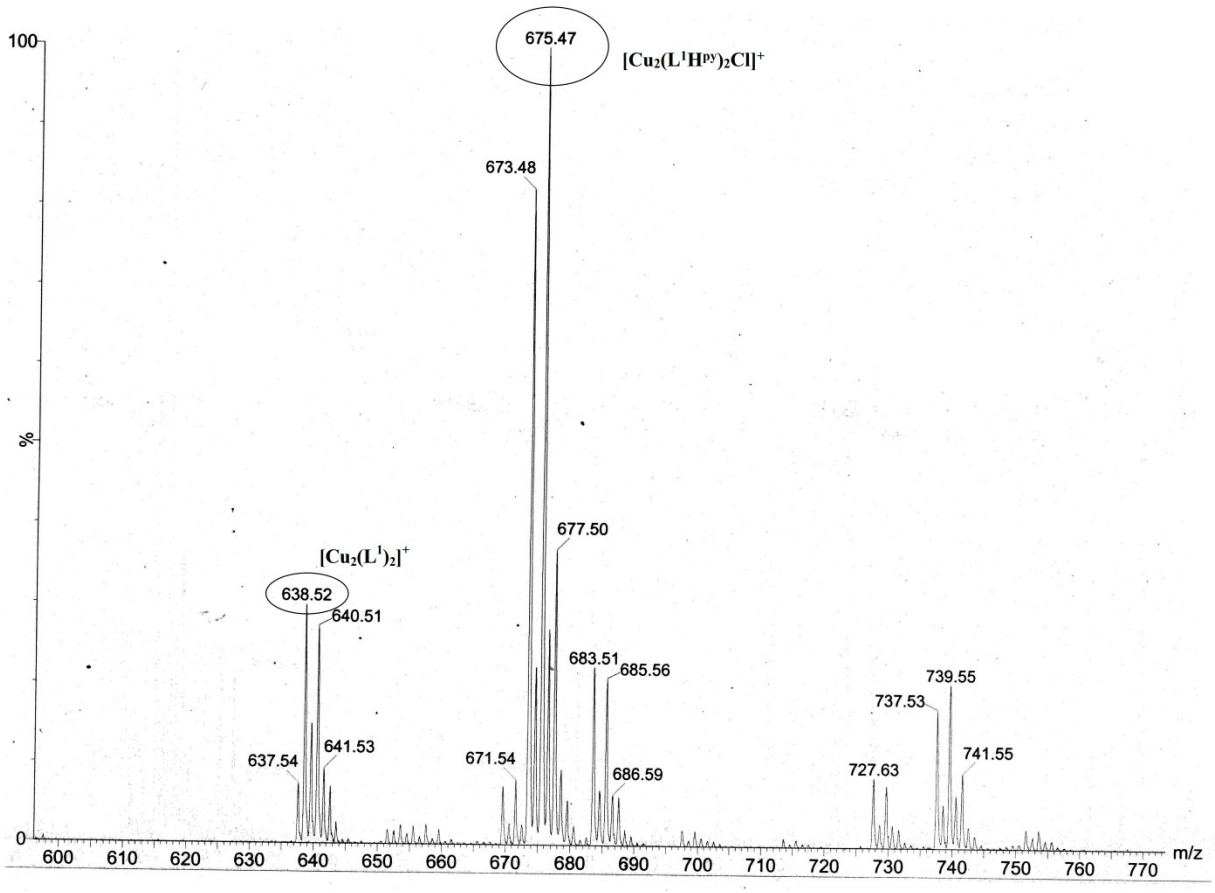

Figure S2: Extended Mass spectrum(in positive mode) of **1** in methanol.

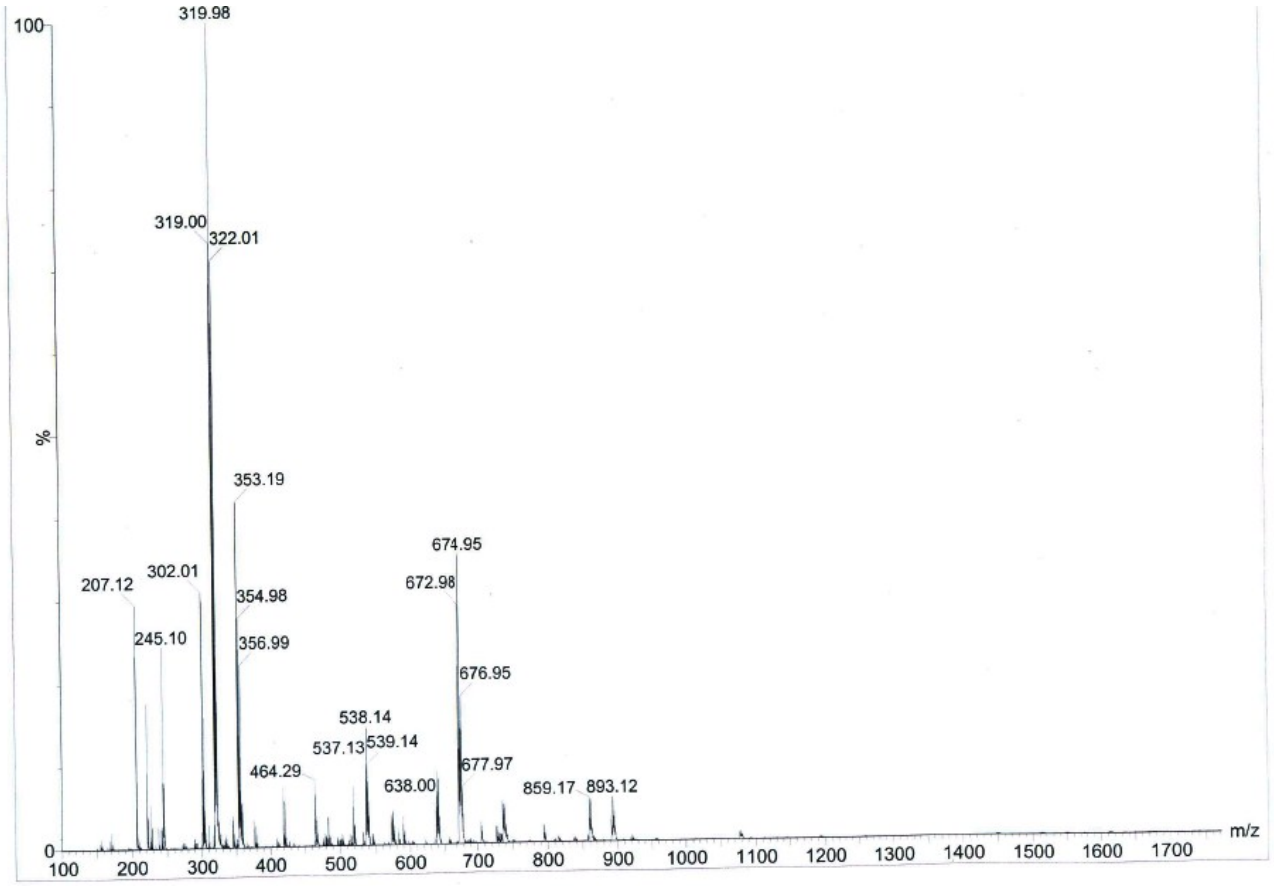

Figure S3: Mass spectrum(in positive mode) of **1** with 3,5-DTBC in methanol solvent.

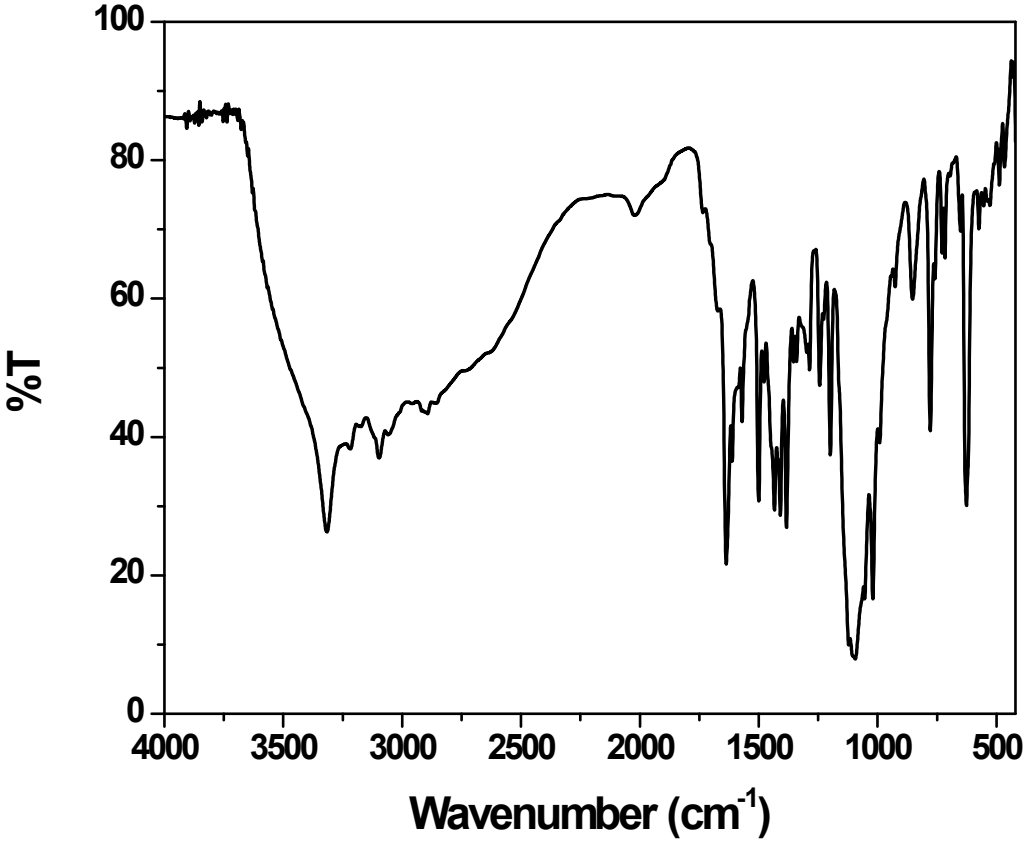

Figure S4: IR of complex **1**.

In the IR spectra of compound **1** a sharp band around 3318 cm^{-1} is assigned to ν_{O-H} vibration of the hydroxymethyl functionality. A band at 3095 cm^{-1} is assigned to the ν_{N-H} vibration of the protonated pyridine nitrogen of pyridoxal. A sharp and strong band at 1635 cm^{-1} appears due to azomethine ($\nu_{C=N}$) stretching. A broad band at 1091 cm^{-1} is characteristic of perchlorate ion.

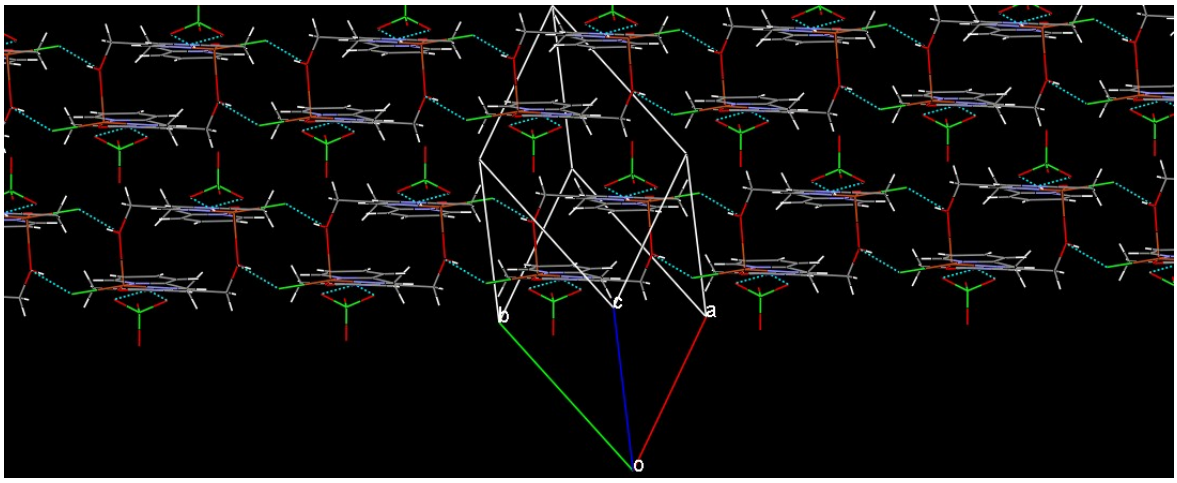

Figure S5: Hydrogen bonded one dimensional chain in **1**.

Each protonated pyridine nitrogen atom remains hydrogen bonded to two oxygen atoms of a perchlorate at x, y, −1+z via N3–H3…O(5) and N3–H3…O(6) (D…A distances are 2.943(4) and 3.017(5)Å respectively ; D–H…A angles are 129(4) and 154(5)° respectively). Each hydroxymethyl –OH group is also involved in complementary H-bonding with a chloride ion of an adjacent unit at 1+x, −1+y, z (D…A distance 3.092 (3)Å, D–H…A angle 159(6)°), whereby each dimer acts as donors as well as acceptors of two H-bonds each, thereby forming a one dimensional chain along [1 −1 0]base vector (Fig. S5)

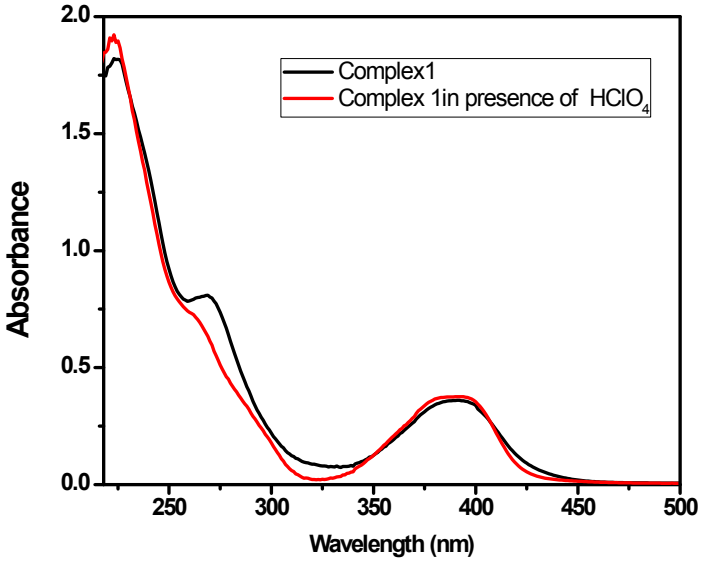

Figure S6: Electronic spectra of **1** in presence of methanolic $HClO_4$.

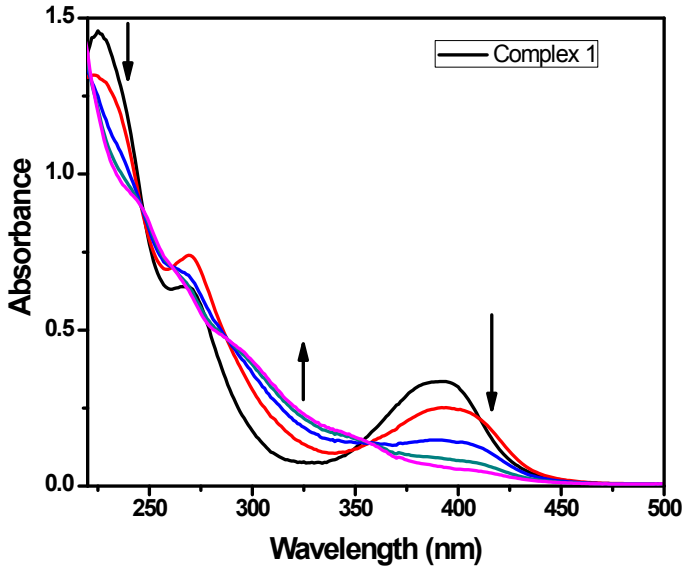

Figure S7: Electronic spectra of **1** in presence of methanolic KOH.

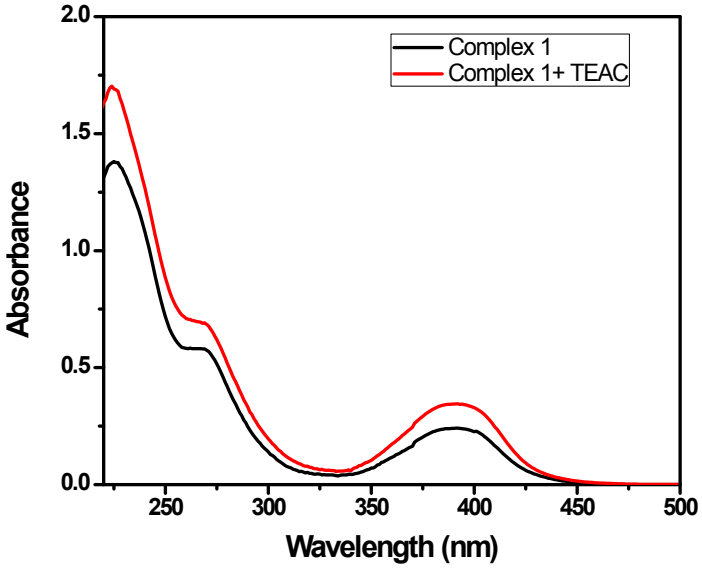

Figure S8: Electronic spectra of **1** in presence of methanolic TEAC.

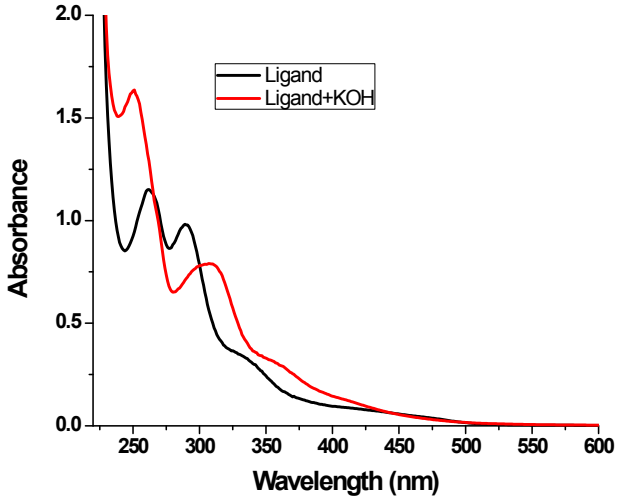

Figure S9: Electronic spectra of L^1H_2 before and after addition of methanolic KOH.

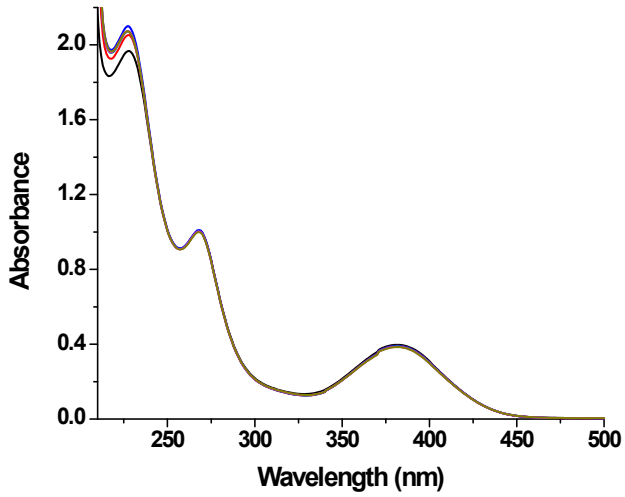

Figure S10: UV-vis spectral changes of complex Cu-5(5×10^{-5} M) in aqueous Tris-HCl medium at pH 7.4, observed at fifteen minute intervals of time.

Description of the EPR spectra:

The electron spin resonance (ESR) spectrum in MeOH frozen solution (77 K) of this compound was recorded at X-band frequency (Figure 4). This spectrum, with $g_{II}>g_{\perp}>$ 2.002, is characteristic of a d_{x2-y2} the ground state for Cu(II) located in a square-based geometry.[1] This is consistent with the SOMO (Fig S11) obtained from DFT calculations. The hyperfine coupling (I_{Cu} = 3/2) is observed in the parallel region. However, the presence of two superimposed signals around g~2 suggests that there are two different mononuclear species in solution. With the aim to confirm this fact a simulation of the experimental spectrum has been carried out with the EasySpin software package.[2]

A quite good simulation was obtained considering two mononuclear entities with some differences in the hyperfine coupling and g parameters: Cu1: $g_{\perp}$ = 2.13, g_{II} = 2.40, A_{II} = 140× 10^{-4} cm^{-1}; Cu2: $g_{\perp}$ = 2.10, g_{II} = 2.30, A_{II} = 107 ×10^{-4} cm^{-1}.

The simulations carried out shown that the shape of the spectra in the g ~ 2 region depends on the ratio between these entities. The best reproduction of the experimental spectra was found for

a Cu1:Cu2 ratio of 3:2. This compares well with the conclusion drawn from the electronic spectra where similar ratio of $[Cu(L^1H^{py})Cl]^+$ and $[Cu(L^1H^{py})(MeOH)]^{2+}$ was deducted in MeOH solution.

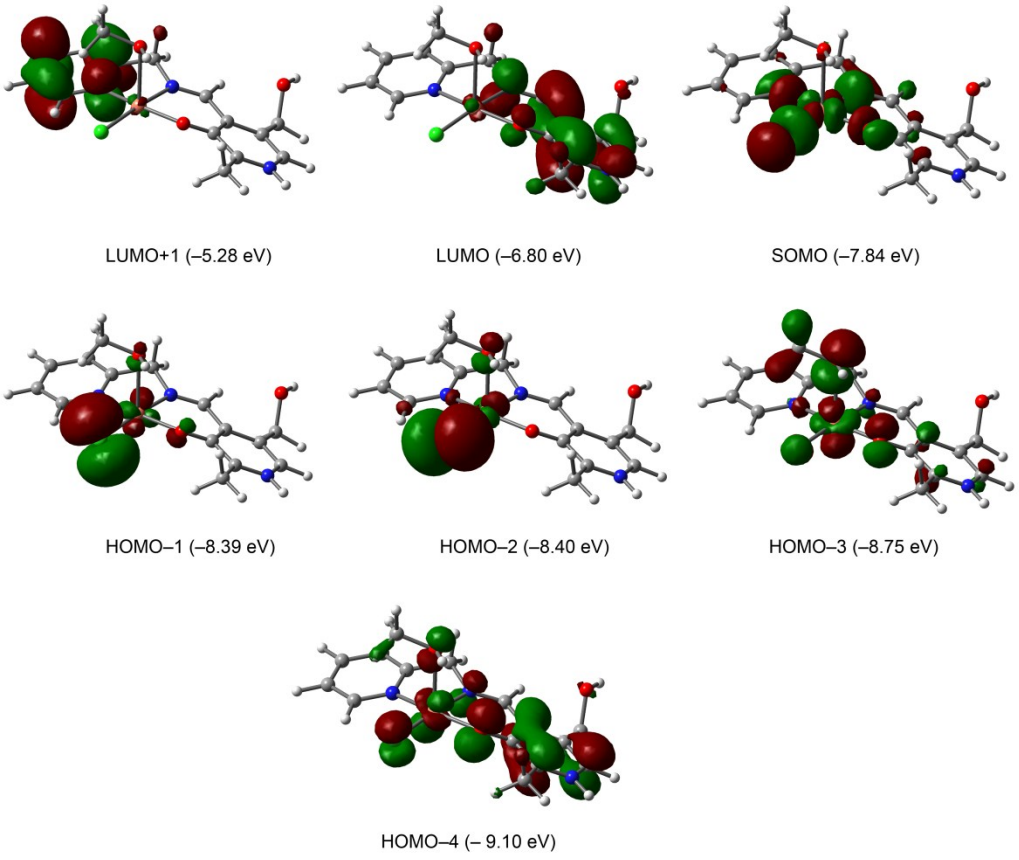

Figure S11: Frontier Orbital of $[Cu(L_1H^{py})Cl(MeOH)]^+$.

Conductivity study

Molar conductivity of compound **1** in MeOH solution was measured at 298 K at ten different concentrations within the range of 2×10^{-4} M to 1×10^{-3} M. The molar conductance value was found to be in the narrow range of 106-110 Ω^{-1} cm^2 M^{-1} (taking molecular weight for the mononuclear species$[Cu(L^1H^{py})Cl]ClO_4$). For tetraethylammonium chloride in the same concentration range the molar conductance value was found to be in the range 80-94 Ω^{-1} cm^2 M^{-1}.This value suggests that compound **1** behaves as a 1:1 electrolyte and the pyridine nitrogen remains protonated in solution and the chloride ion remains coordinated to Cu(II).

Cyclic voltametry:

In Cyclic voltammetric studies of **1** in MeCN solution, on the negative side of the reference electrode the compound shows an irreversible reductive wave at −0.26 V (Fig. 3), which is assigned to Cu(II)/Cu(I) reduction. On the positive side, a weak oxidative response at 0.78 V (ΔEp= 120 mV) is observed, however its current height is so small compared to that of the reductive peak at −0.26 V, it can be neglected as a minor decomposition product. At more negative potential at −0.61 V another irreversible wave, which on scan reversal shows strong anodic stripping current at −0.22 V is assigned to Cu(I)/Cu(0) reduction (Fig. S11).

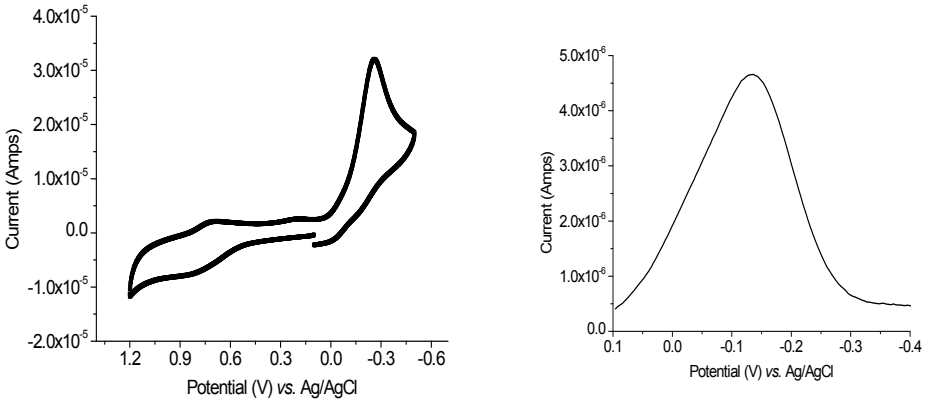

Figure S12: Cyclic Voltammogram and Differential Pulse Voltammogram of compound **1** in MeCN at GC electrode.

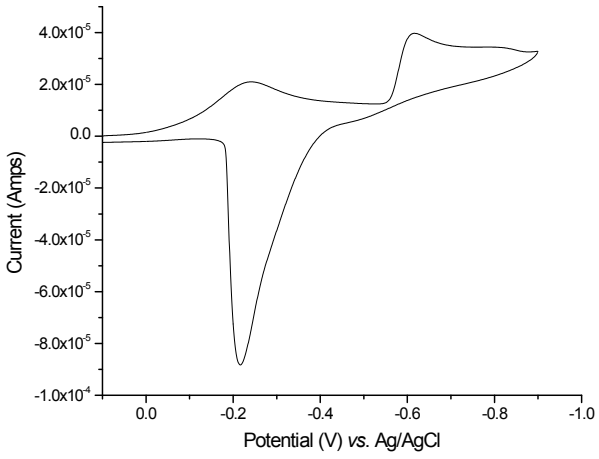

Figure S13: CV of Complex **1** at GC electrode.

Table S1: Comparison of kinetic parameter for catecholase by complex **1**

Nature of plot	$V_{max}(Mmin^{-1})$	$K_M(M)$	$k_{cat}(h^{-1})$
Lineweaver-Burk Plot	1.15×10^{-1}	3.45×10^{-3}	3.46×10^{5}
Rate vs [Substrate] Plot	1.15×10^{-1}	3.51×10^{-3}	3.40×10^{5}

Table S2: Kinetic Data for Catecholase-like Activity of Different Mono- and DinuclearCu(II) compounds

Complexes	solvent	$k_{cat}(h^{-1})$	Ref.
$[Cu_2L^2_2(ClO_4)_2]$	MeOH	93.6	3
$[Cu_2L^2_2(OH)]ClO_4$	MeOH	233.4	3
$[Cu_2(H_2L^3)(OH)(H_2O)(NO_3)](NO_3)_3 \cdot 2H_2O$	MeOH	3.24×10^4	3
$[Cu(HL^4)(H_2O)(NO_3)]_2(NO_3)_2 \cdot 2H_2O$.	MeOH	1.44×10^4	4
$[Cu(L^5)(H_2O)(NO_3)]_2$.	MeOH	1.08×10^4	4
$[Cu_2(L^6)(OH)(H_2O)_2](NO_3)_2$.	MeOH	1.44×10^4	4
$[Cu_2(L^7)(N_3)_3]$.	MeOH	2.88×10^4	4

HL^2 = 2-[[2-(diethylamino)ethylamino]methyl]-phenol
H_3L^3 = 2,6-bis((E)-(2-(piperazin-1-yl)ethylimino)methyl)-4-methylphenol
H_2L^4 = 3-((E)-(2-morpholinoethylimino)methyl)-2-hydroxy-5-methylbenzaldehyde
H_2L^5 = 3-((E)-(3-morpholinopropylimino)methyl)-2-hydroxy-5-methylbenzaldehyde

HL^6 = 2,6-bis((E)-(2-pyrrolidin-1-yl)ethylimino)methyl)-4-methylphenol
HL^7= 2,6-bis((E)-(3-morpholinopropylimono)methyl)-4-methylphenol

DFT study of the optimized structures of the intermediates in the catalytic reaction scheme

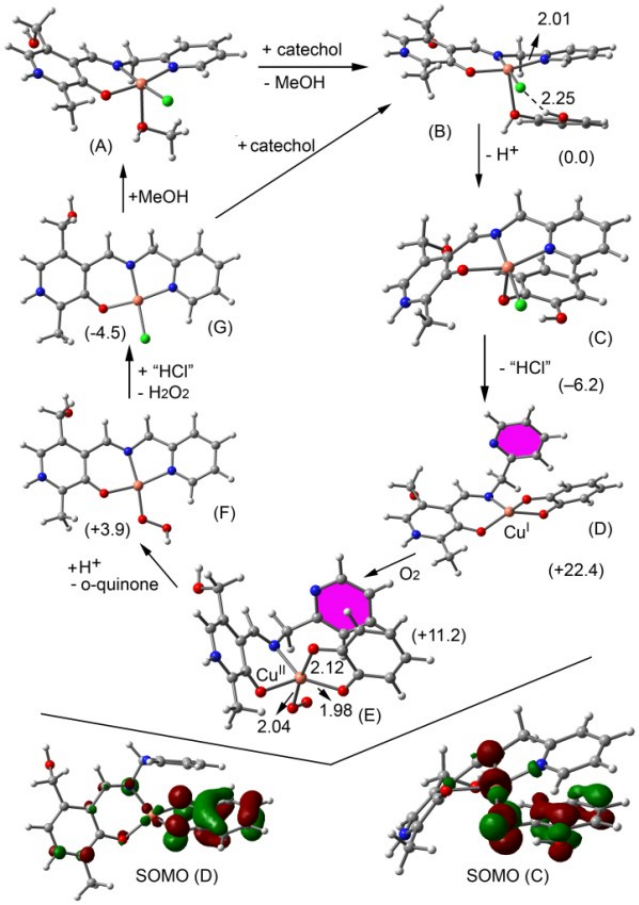

Figure S14: BP86/def2-TZVP optimized structures of A-E intermediates of the catalytic cycle. Distances are in Å. The hydrogen atoms have been omitted for clarity apart from the OH group of the coordinated catechol to differentiate it from the anionic oxygen atom. Energies in kcal/mol of the different intermediates relative to B are given in parenthesis.

Fig. S13 we show the optimized geometries of complexes **A**–**G**. It can be observed that the Cu–monocoordinated catechol molecule (in complex **B**) forms a H-bonding interaction with the chlorido ligand (Cl···H distance 2.25 Å) by means of the uncoordinated OH group. This interaction is important to fix the initial geometry of the catechol in the complex and

increases the acidity of the hydroxyl H atom. In compound **C**, both the metal center and the π-system catecholate ligand contribute to the SOMO, which is also shown in Figure 8, in agreement with the proposed electron transfer from the chatecolate to the Cu metal center (see scheme 1). The elimination of "HCl" yields intermediate **D** where the pyridine moiety (highlighted in fuchsia) is not coordinated to Cu. The pseudo-tetrahedral coordination around the metal center agrees well with the d^{10} configuration of the metal center. Moreover, the SOMO representation of **D** further confirms the oxidation state of Cu (see Figure 8), since the unpaired electron is basically located at the catechol ring with a minimum contribution of the atomic orbitals of Cu. It should be mentioned that this is likely the rate determining step, since the transformation of **C** to **D** has an energy cost of $\Delta E_{\mathbf{C}\rightarrow\mathbf{D}}$ =28.6 kcal/mol at the PB86-D3/def2-TZVP level of theory in MeOH. The transformation of **D** to **E** involves the incorporation of molecular oxygen and the concomitant oxidation of the Cu(I) ion. In complex **E** the Cu(II) metal center adopts a trigonal-bipyramidal coordination. The reaction energy of this step is favorable $\Delta E_{\mathbf{D}\rightarrow\mathbf{E}}$ = –11.2 kcal/mol. Upon the second electron transfer from the semibenzo-*o*-quinone to the Cu–O–O$^{\bullet}$ moiety, the *o*-benzoquinone is released and the pyridine ring coordinates to the Cu again. Finally, the complexation of the chlorido ligand and the generation of hydrogen peroxide complete the catalytic cycle. This mechanistic step is also energetically favorable since $\Delta E_{\mathbf{F}\rightarrow\mathbf{G}}$ = –8.4 kcal/mol.

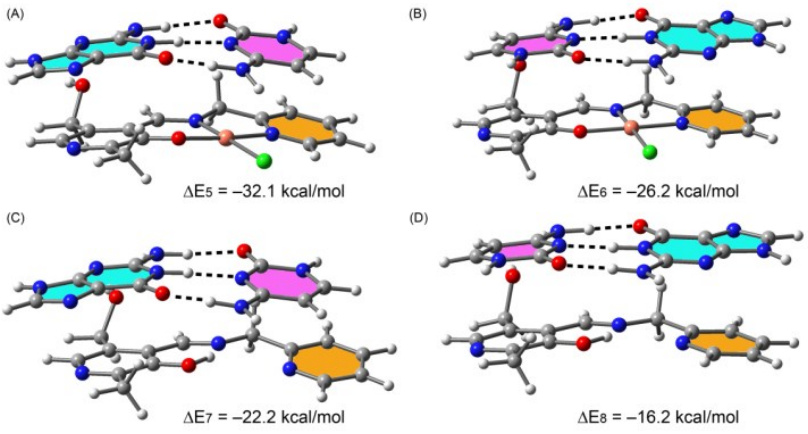

Figure S15: PB86-D3/def2-TZVP optimized geometries and interaction energies of G–C base pair complexes with the monomeric form of **1**.

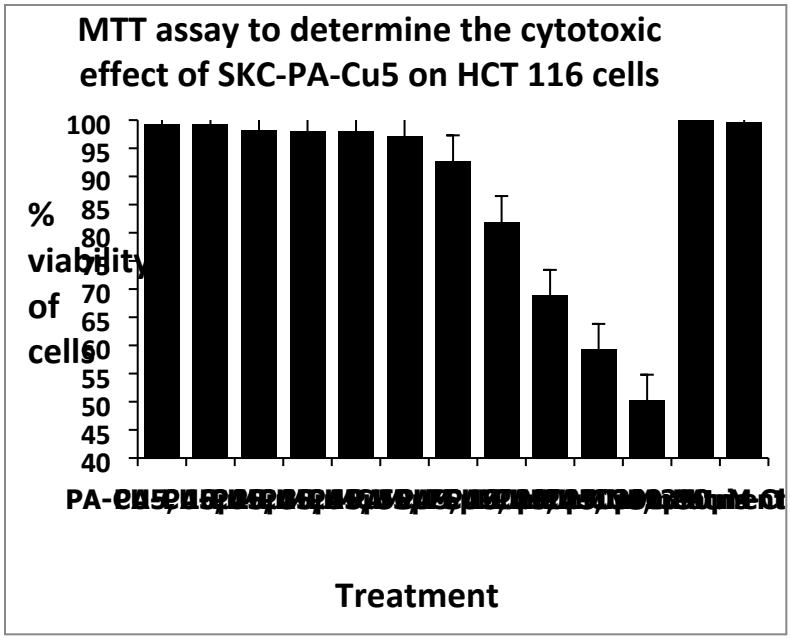

Figure S16: MTT assay of cytotoxic effect of 1 on HCT 116 cells

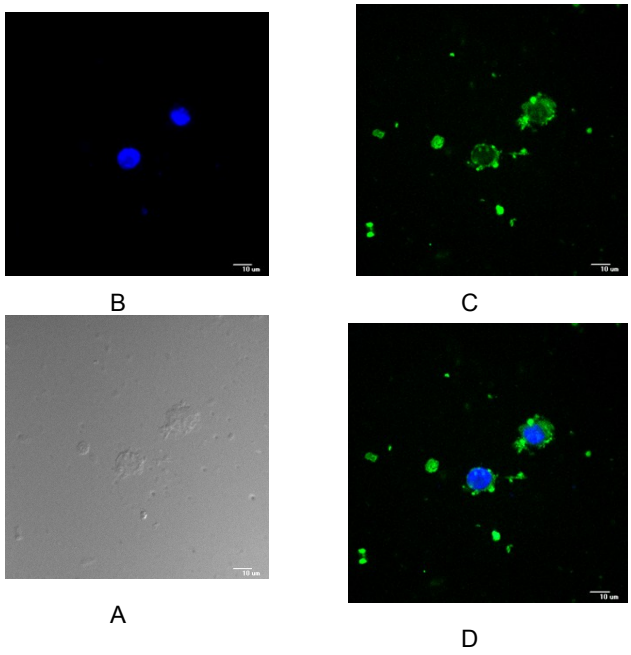

Figure S17: Confocal microscopic images of HeLa cells, All images were acquired with a 100× objective lens. (a) Bright field image of cells (b) Fluorescence images of cells without probe (complex **1**), nuclei counterstained with Hoechst 33342 Fluorescent Stain (1µg/mL) (c) Fluorescence images of cells with probe (complex **1**) excited at 405 nm (d) Overlay image of (b) and (c)

References:

1. (a) B. J. Hathaway, D. E. Billing, *Coord. Chem. Rev.* 1970, **5**, 1. (b)B. J. Hathaway, M. Duggan, A. Murphy, J. Mullane, C. Power, A. Walsh, B. Walsh, *Coord. Chem. Rev.* 1981, **36**, 267.

2. S. Stoll, A.Schweiger, *J. Magn. Reson.* 2006, **178**, 42.

3. A. Biswas, L.K. Das,G. B. Drew,D. C.Michael, A. Ghosh, *Inorg. Chem.*, 2012, **51**, 10111.

4. K. S.Banu, T. Chattopadhyay, A. Banerjee, S. Bhattacharya, E. Suresh, M.Nethaji, E.Zangrando, D.Das, *Inorg. Chem.*,2008, **47**, 7083.